UNCLASSIFIED

DEFENCE RESEARCH ESTABLISHMENT
CENTRE DE RECHERCHES POUR LA DÉFENSE
VALCARTIER, QUÉBEC

DREV-TM-2000-032

Unlimited Distribution/Distribution illimitée

A RANGE-GATED INTENSIFIED SPECTROGRAPHIC IMAGER: AN INSTRUMENT FOR ACTIVE HYPERSPECTRAL IMAGING

by

Jean-Robert Simard, Pierre Mathieu, Georges Fournier and Vincent Larochelle
And
S.K. Babey, ITRES Research Ltd.

May/mai 2000

Approved by/approuvé par

Gabriel Ait

Section Head/Chef de section

4 May 2000

Date

SANS CLASSIFICATION

102-00848/

WARNING NOTICE

The information contained herein is proprietary to Her Majesty and is provided to the recipient on the understanding that it will be used for information and evaluation purposes only. Any commercial use, including use for manufacture, is prohibited. Release to third parties of this publication or of information contained herein is prohibited without the prior written consent of DND Canada.

© Her Majesty the Queen in Right of Canada as represented by the Minister of National Defence, 2000

ABSTRACT

Hyperspectral imaging has demonstrated impressive capabilities in airborne surveys, particularly for mineral and biomass characterisations. Based on this success, it is believed that other applications like search and rescue operations, and detection/identification of various ground military targets could greatly benefit from this technology. The strength of hyperspectral imaging comes from the access to another dimension of information: the spectral content of the detected return signal for each spatial pixel. In the case of conventional hyperspectral imaging, the return signal depicts the spectral reflectance of the day irradiance from the scene within the field of view of each pixel. However, by inserting a range-gated intensifier into a hyperspectral camera and by combining the camera with selected pulsed lasers, it becomes possible to relate the returned spectral information to specific light/matter interactions like induced fluorescence. This new technique may be referred to as "active hyperspectral imaging". Among its advantages, this approach is independent of the ambient lighting conditions and can be customised in excitation wavelengths. Moreover, by using a range-gated intensified camera, it is possible to survey limited areas with a significant increase in signal-to-noise ratio. A camera of this type has been built by our group in collaboration with private industry and is described in this document. The internal design of the camera is discussed, new issues concerning the calibration of the camera are depicted and a model based on signal-to-noise ratio analysis is presented. From the fluorescent characteristics of surrogate land mines measured in the laboratory, this model is used to predict the capabilities of detecting surface-laid mines from an aerial platform.

RÉSUMÉ

L'imagerie hyperspectrale a démontré son plein potentiel en surveillance aérienne, plus particulièrement pour la caractérisation de la biomasse et des ressources minéralogiques. Il est donc raisonnable de croire que d'autres applications pourraient tirer profit de ce potentiel : les opérations de recherche et sauvetage, et la détection et l'identification de diverses cibles militaires. La puissance de cette technique repose sur une nouvelle dimension de l'information : le contenu spectral du signal mesuré pour chaque pixel spatial de la scène sous observation. Dans le cas de l'imagerie hyperspectrale conventionnelle, ce signal est constitué de la réflexion spectrale de la radiation solaire qui éclaire la scène. Toutefois, il est possible d'améliorer un imageur hyperspectral traditionnel pour soutirer des renseignements supplémentaires en lui ajoutant deux composantes : 1) un intensificateur d'image à ouverture contrôlée dans le temps et 2) une source laser pulsée, synchronisée avec l'intensificateur. Il devient alors possible de provoquer des interactions laser-matière (par ex. fluorescence induite). On peut désigner cette technique comme l'*imagerie hyperspectrale active*. Celle-ci présente l'avantage d'être indépendante de la lumière ambiante et de pouvoir choisir la longueur d'onde ou le spectre d'excitation ou d'illumination. De plus, grâce à une technique de crénelage et de synchronisme entre la caméra intensifiée et le laser pulsé, on peut limiter en distance la tranche spatiale inspectée, ce qui augmente grandement le rapport signal/bruit. Un système d'imagerie hyperspectrale active a été construit au CRDV en collaboration avec l'industrie privée. Ce document en examine la conception, et en décrit les aspects nouveaux découlant de l'étalonnage de la caméra. Il présente également un modèle numérique de l'analyse du rapport signal/bruit. Validé par des mesures de caractéristiques de fluorescence de mines inertes, ce modèle est utilisé pour prédire le potentiel de cette technique pour la détection, depuis une plate-forme aérienne, de mines déposées en surface.

This page is left blank

This page is left blank

TABLE OF CONTENTS

ABSTRACT/RÉSUMÉ i
EXECUTIVE SUMMARY v
1.0 INTRODUCTION 1
2.0 DESCRIPTION OF THE INTENSIFIED SPECTROGRAPHIC IMAGER 2
3.0 MODELLING OF INTENSIFIED HYPERSPECTRAL IMAGING 3
4.0 SIGNAL-TO-NOISE FUNDAMENTALS 8
5.0 ABSOLUTE CALIBRATION OF THE INTENSIFIED CASI 10
6.0 FLUORESCENT CHARACTERISTICS OF TYPICAL SURROGATE MINES 12
7.0 SURFACE-LAID MINES DETECTION MODELLING 14
8.0 CONCLUSION 15
9.0 REFERENCES 16
10.0 FIGURES AND TABLES 17

FIGURES 1 to 5

TABLE I

This page is left blank

This page is left blank

EXECUTIVE SUMMARY

Remote sensing has demonstrated countless successes in diverse applications covering agricultural survey, resource monitoring, terrain analysis, object detection/classification, material characterisation and rogue nations surveillance. Driven by Canada's vast territory and its long coastline, the Canadian Forces have shown great interest in new developments related to remote sensing. In active imaging, the ALBEDOS and ELVISS programs are examples of a new technology developed in support of these requirements. Active imaging has performed particularly well in the detection and recognition of objects and backgrounds under limited visibility conditions, circumstances of prime importance for military imaging applications. Another technology that has shown impressive capabilities in the last few years is hyperspectral imaging. This technique involves the detection and recognition of targets based not only on their spatial aspects but also on their spectral characteristics. Beside their shapes, the spectral content of the light returned by objects and backgrounds is rich in information and can be used for discrimination and identification. With hyperspectral imaging, one can acquire this colour-embedded information with a sufficient spectral resolution in order to detect/identify target specific signatures. In the visible, one deficiency of this technique is that it relies on natural ambient lighting. In order to reduce this limitation, the possibility of replacing the ambient light by an artificial source is investigated. If this source is white or broadband, then the reflectance of the target is questioned. On the other hand, with a selected monochromatic source, a light-matter interaction (induced fluorescence) specific to the target of interest may be produced and remotely detected. The acquisition of spectrally distributed information from a target using an artificial light source is referred to as active hyperspectral imaging.

The work described here is based on a commercial hyperspectral camera, the second generation Compact Airborne Spectrographic Imager (CASI-2) designed and built by ITRES Research Limited. The CASI-2 has been modified by the insertion of a range-gated intensifier. This document reports the characteristics and technical specifications of this modified instrument. An absolute calibration method taking into account the variable gain of the intensified hyperspectral camera is depicted. Then, a detailed model based on a signal-to-noise ratio analysis is proposed to predict the capabilities of the instrument in active and passive modes (i.e., with and without the use of an artificial light source) as a function of the spectral characteristics of the target to detect/identify. As an example, this model is applied to the detection of surface-laid mines by induced fluorescence using a UV light source. In order to do so, the fluorescence characteristics of surrogate mines are measured in the laboratory and inserted in the model. Then, a signal-to-noise ratio, from which a probability of detection and false alarm rate can be derived, is predicted by the model as a function of the area scanning speed of the scene.

1.0 INTRODUCTION

In the last few years, hyperspectral imaging has shown important capabilities in civilian applications such as agriculture monitoring (Ref. 1), terrain categorisation (Ref. 2) and terrain hydrodynamic characterisation (Ref. 3). Also, it has demonstrated significant potential in surveillance application associated with military activities like the detection of surface-laid/buried mines (Refs. 4 and 5) and improved military surveillance applications (Refs. 6 and 7). The two main requirements for these applications are the need for a well characterised natural irradiance of the scene (Ref. 1) and a precise calibration of the parasitic signals of the detector for scenes with low radiance (Ref. 8). One way to relax these requirements is to integrate a range-gated intensified hyperspectral camera with a pulsed artificial light source and to collect the resulting spectral response of the scene. This technique is referred to as active hyperspectral imaging. The artificial light source can be broadband in the visible. In this case, the reflectance of the scene is produced with a well-characterised irradiance at the scene, independently of the ambient natural radiance. Another approach is to irradiate the scene with a selected monochromatic light source. Here, specific light-matter interactions generated at the scene can be spectrally or dynamically (fluorescent time decay) correlated with the characteristics of the target to detect/identify. Furthermore, with the intensified capabilities, a camera of this type does not have to be operated anymore with a low number of electrons per CCD pixel, a common situation when only the radiance of a line of the scene is recorded at a times over the whole CCD array. With this option, additive parasitic noises like the CCD noise floor can be neglected most of the time, which leaves the shot noise associated with the collected radiance as the main limiting noise source.

This document presents an intensified spectrographic imager developed under a contract supervised by DREV. Its design and specifications are reported and a calibration procedure is detailed. A model based on a signal-to-noise ratio analysis is proposed to provide a preliminary assessment on the capabilities of using active (or passive, to a certain extent) hyperspectral imaging techniques in surveillance scenarios. As an example, this model is applied to the detection of surface-laid mines by the hyperspectral

detection of induced fluorescence. To perform this evaluation, the fluorescent properties of surrogate mines were measured in laboratory. Then, based on representative parameters associated with a scenario where the active hyperspectral detection is performed from an aerial platform, a predicted signal-to-noise ratio is derived as a function of the area scan speed.

This work was carried out at DREV between July 1999 and February 2000 under Work Unit 3da29: "Active Hyperspectral Imaging".

2.0 DESCRIPTION OF THE INTENSIFIED SPECTROGRAPHIC IMAGER

The intensified hyperspectral camera has been developed by modifying a commercial off-the-shelf product, the Next-Generation Compact Airborne Spectrometric Imager (CASI-2) developed by ITRES Research Ltd.[1] (see Ref. 9). The modification consisted in inserting a micro-channel plate (MCP) between the CCD and the focal plane of the camera lens (see Fig. 1). This modification did not change the dimension of the camera head (about 1/3 cubic foot), but necessitated an additional power supply. The resulting intensified CASI is completely controlled by a PC based data processing station. The hyperspectral imaging process is produced by a push broom method where the spatial image of the scene is acquired one line at a time. The complete image of the scene is made by translating (or panning) this imaged line over the scene. The imaged line is produced by inserting a narrow slit (15 μm in width) at the focus of the collecting lens. The radiant energy passing through the slit is collected by the collimator lens and diffracted by a grating. Then, a camera lens collects the diffracted light and forms spectrally dispersed images of the entrance slit on the photocathode of the intensifier. Later in this document, we will refer to the spatial and the spectral information associated with the imaged line as being along the rows and the columns of the CCD, respectively. The photoelectrons resulting from the spectral irradiance of the photocathode are amplified by the MCP and are transformed into photons by a phosphor screen (see Fig. 2). Finally, this phosphorescence is collected at the CCD via a fiber optic taper. The level

[1] ITRES Instruments Inc., Suite 155, 2635-37th Avenue NE, Calgary (AB) T1Y 5Z6, Canada.

of the MCP gain is set via an eight-bit register (0-255). There is unity magnification between the slit and the photocathode planes, and between the photocathode and the CCD planes. The length of the entrance slit corresponds to a row of 512 pixels on the CCD. The columns (or binned columns) associated with these pixels are referred to as look directions. In addition to these 512 pixels, another 100 pixels (for a total of 612 pixels per row) may be used to correct the dark current, the scattered light, or other parasitic signals. A total of 288 pixels per column is available for the spectral information: this corresponds to a spectral interval ranging from 373 to 918 nm. A maximum of 101 columns (or look directions), each containing the 288 spectral samples, can be collected within a minimum integration time of about 150 ms. By switching to hard disk (versus tape) recording and by upgrading the readout firmware, it is expected that this minimum integration period will be reduced below 100 ms. Furthermore, the columns or the rows can be binned in order to expand the width of the swath or to reduce the minimum integration time at the expense of the spatial or spectral resolution. Additional specifications on the intensified CASI can be found in Table I.

3.0 MODELLING OF INTENSIFIED HYPERSPECTRAL IMAGING

The signals generated at the CCD can be classified in two types: signals that are dependent on the collected radiant energy and those that are not. Examples of the latter are the CCD dark current and electronic offset. Little will be said on these signals in the present paper. For those interested in this aspect of the camera are invited to consult Reference 8. Even if not detailed, all experimental acquisitions made with the intensified CASI and reported in this document have been corrected accordingly to Ref. 8. Based on the direct spatial correspondence (and the linear relationship) between the signal generated at the CCD and the radiant energy incident on the photocathode, the radiance dependent signal at the photocathode can be expressed as

$$n_{i,j}^{tot} = n_{i,j}^{SC} + n_{i,j}^{SL} + n_{i,j}^{FSS} . \qquad (1)$$

In this equation, $n_{i,j}^{SC}$, $n_{i,j}^{SL}$, and $n_{i,j}^{FSS}$ are radiant energies originating from the scene, from the light scattered within the instrument, and from the frame shift smear, respectively. Indices i and j correspond to a specific area element on the photocathode and,

equivalently, to a look direction (spatial information) and to a spectral interval (spectral information), respectively. These indices are also related to (binned) column(s) and (binned) row(s) on the CCD, respectively. The contributions of $n_{i,j}^{SL}$ and $n_{i,j}^{FSS}$ to the collected signal can be adequately corrected using a method described in Reference 8. Once the collected signal is corrected for these parasitic contributions, the remaining signal, $n_{i,j}^{SC}$, is related to $E_{i,j}^{SC}$, the spatial and spectral distributions of the specific intensity of the spectral radiant energy of the imaged line at the scene. Based on radiometric considerations where the cosine of the incident signal at the collecting lens is neglected (Ref. 10), this relation is quantitatively defined as

$$n_{i,j}^{SC} = E_{i,j}^{SC} \frac{A_{cl}}{r_i^2} r_i^2 \Omega_i^{IFOV} t_{i,j}^{a} t_{i,j}^{o} \eta_{i,j}^{g} , \qquad (2)$$

where A_{cl} is the area of the collecting lens, r_i is the range between the position along the imaged line at the scene identified by index i and the collecting lens, and $t_{i,j}^{a}$, $t_{i,j}^{o}$, $\eta_{i,j}^{g}$ are the transmission of the atmosphere, the transmission of the optics, and the diffraction efficiency of the grating for signal reaching position i,j on the photocathode, respectively. Because of the unitary magnification between the CCD and the photocathode planes, the parameter Ω_i^{IFOV} corresponds to the instantaneous field of view (FOV) of the collecting system. It corresponds to the FOV of several CCD pixels or a single pixel according as CCD columns are binned or not. It is useful to introduce the following basic optical definitions in Equation 2,

$$\Omega_i^{IFOV} = \frac{A_i^{IFOV}}{f^2}, \quad A_{cl} = \frac{\pi}{4} \frac{f^2}{F\#^2}, \qquad (3)$$

where A_i^{IFOV} is the sensitive area of the (binned) pixel(s) along a row of the CCD, f and F# are the focal length and the f-number of the collecting lens, respectively. Once these definitions are substituted, Equation 2 is reduced to

$$n_{i,j}^{SC} = \frac{\pi}{4} \frac{A_i^{IFOV}}{F\#^2} t_{i,j}^{a} t_{i,j}^{o} \eta_{i,j}^{g} E_{i,j}^{SC} = C_{i,j} E_{i,j}^{SC} . \qquad (4)$$

Here, $C_{i,j}$ represents the collection efficiency and regroups the parameters defining the fraction of emitted photons at the scene that reaches the area corresponding to the CCD

IFOV at the photocathode during the time of integration. It is important to note that the signal collected is not explicitly related to the size of the collecting lens. This results from the optical definitions previously introduced which couple the size of the lens to the IFOV of the imaging system. This coupling may be cancelled by keeping the IFOV constant as the size of the lens is increased. This may be done by binning columns (or view directions) at the CCD. However, because of the single dimensional property associated with the entrance slit, common with most push broom methods, only a linear increase of the signal with the diameter of the collecting lens can be expected with this process for passive imaging systems. On the other hand, a quadratic relation between the diameter of the collecting lens and the signal collected may be expected for active systems if the artificial irradiation is narrowed with the imaged line as the lens diameter is increased, while keeping the swath on the ground constant. With the signal at the photocathode defined by Equation 4, the corresponding signal detected by the CCD, $n_{i,j}^{CCD}$, is given by

$$n_{i,j}^{CCD} = \eta_{i,j}^{CCD}\ T_{i,j}^{FB}\ \eta_{i,j}^{PS}\ G_{i,j}\ (\eta_{i,j}^{PC} n_{i,j}^{SC} + \varepsilon_{EBI}\Delta t) \qquad (5)$$

where $\eta_{i,j}^{PC}, G_{i,j}, \eta_{i,j}^{PS}, T_{i,j}^{FB}$ and $\eta_{i,j}^{CCD}$ are the quantum efficiency of the photocathode, the gain of the MCP, the quantum efficiency of the phosphor screen, the transmission of the fiber bundle and the quantum efficiency of the CCD corresponding to the i^{th} IFOV and j^{th} spectral interval, respectively. The equivalent background illuminance, ε_{EBI}, is introduced here in photons per second for the area on the photocathode corresponding to the position i,j. Δt is the integration time. The last term of this equation takes into account the self-emitted electrons associated with the photocathode substrate. This parasitic signal is expected to become important only under very low collected spectral radiant energy situations which occur under low sun radiance (like at night) when the camera is used as a passive hyperspectral imager, or with long gating periods when used as an active hyperspectral imager.

In the previous paragraph, expressions were developed to define the signal expected with an hyperspectral camera like the intensified CASI as a function of several parameters. To refine further this model, expressions have to be developed for the noise

and ultimately, the signal-to-noise ratio (SNR). From standard intensified CCD noise analysis (Ref. 10), the noise at the CCD is defined as

$$\langle n^2_{i,j/CCD} \rangle = (\eta^{CCD}_{i,j}\, T^{FB}_{i,j}\, \eta^{PS}_{i,j}\, G_{i,j})^2\, k\, \langle n^2_{i,j/ph\text{-}SHOT} \rangle + \langle n^2_{i,j/CCD\text{-}SHOT} \rangle + \langle n^2_{i,j/FLOOR} \rangle , \qquad (6)$$

where k represents the intensifier SNR degradation factor and is reported to be of the order of 1.8 (can vary with the MCP applied bias voltage) (Ref. 11); $\langle n^2_{i,j/FLOOR} \rangle$ is the standard CCD floor noise combining the reset noise, the on-chip and off-chip amplifier noises and the A/D conversion noise; $\langle n^2_{i,j/ph\text{-}SHOT} \rangle$ is the photon shot noise at the photocathode given (based on Poisson statistics) by $\eta^{PC}_{i,j} n^{SC}_{i,j} + \varepsilon_{EBI} \Delta t$; and $\langle n^2_{i,j/CCD\text{-}SHOT} \rangle$ is the CCD shot noise also defined from Poisson statistics as

$$\langle n^2_{i,j/CCD\text{-}SHOT} \rangle = \eta^{CCD}_{i,j}\, T^{FB}_{i,j}\, \eta^{PS}_{i,j}\, G_{i,j} (\eta^{PC}_{i,j} n^{SC}_{i,j} + \varepsilon_{EBI} \Delta t) + n^{CCD\text{-}dark}_{i,j} , \qquad (7)$$

where $n^{CCD\text{-}dark}_{i,j}$ is the number of electrons generated by the CCD dark current. All these noise definitions are developed for the i^{th} look direction and the j^{th} spectral interval. In these expressions, it is assumed that the pattern noise has been taken care of by a nonuniform responsivity correction.

Finally, one parameter needs to be further developed to complete this model: the spatial density of the spectral radiant energy detected from the scene, $E^{SC}_{i,j}$. This parameter results from the integration of the spectral radiance seen by the IFOV during the scan of the camera slit imaged at the scene and over the data acquisition period of the camera. In order to obtain a versatile expression for this parameter, it is necessary to introduce two additional FOV related parameters: the dynamic and the target FOV. The dynamic FOV is the solid angle associated with the area of the scene scanned by the IFOV during the integration period of the camera. Similarly, the target FOV is the solid angle associated to the target of interest. This last definition is specially interesting for optimised detection schemes. For these scenarios, it is usual to apply a convolution onto the acquired image with a window equivalent to the target of interest in order to maximise the signal to detect. With these definitions, it is now possible to define three types of spectral radiant energy which contribute to $E^{SC}_{i,j}$, that is

$$E^{SC}_{i,j} = E^{T}_{i,j} + E^{BR}_{i,j} + E^{BF}_{i,j} , \qquad (8)$$

where $E_{i,j}^{T}$ is the collected signal associated with the spectral reflectance of the surrounding natural radiant energy (for passive hyperspectral imaging) or the laser-induced fluorescence (for active hyperspectral imaging) when the IFOV is on the target; $E_{i,j}^{BR}$ is the collected signal associated with the background spectral reflectance of the surrounding natural radiant energy when the IFOV is off the target; and $E_{i,j}^{BF}$ is the collected signal associated with the laser induced fluorescence of the background material when the IFOV is not on the target (present only with active hyperspectral imaging). In Equation 8, only $E_{i,j}^{T}$ is the signal of interest. In the best scenarios, $E_{i,j}^{BR}$ and $E_{i,j}^{BF}$ can be uncoupled from $E_{i,j}^{T}$ but are still major noise contributors. Based on these definitions and on basic concepts of radiometry, these three parameters can be defined as

$$E_{i,j}^{BR} = \frac{1}{2\pi} I_{i,j} R_{i,j}^{B} \chi_i^{B} \Delta t \qquad \text{(passive)}, \tag{9}$$

$$E_{i,j}^{BF} = \frac{e_{\lambda_0} \Phi_i^{IFOV} \chi_i^{B}}{r_i^{2}\, \Omega_i^{IFOV}} \frac{\Psi_B^{\lambda_0}}{4\pi} \zeta_{B,j}^{\lambda_0} t_{i,\lambda_0}^{a} = Q_{i,\lambda_0} \chi_i^{B} \Psi_B^{\lambda_0} \zeta_{B,j}^{\lambda_0} \qquad \text{(active)}, \tag{10}$$

$$E_{i,j}^{T} = \begin{cases} \dfrac{1}{2\pi} I_{i,j} R_{i,j}^{T} \chi_i^{T} \Delta t & \text{(passive)} \\ \dfrac{e_{\lambda_0} \Phi_i^{IFOV} \chi_i^{T}}{r_i^{2}\, \Omega_i^{IFOV}} \dfrac{\Psi_T^{\lambda_0}}{4\pi} \zeta_{T,j}^{\lambda_0} t_{i,\lambda_0}^{a} = Q_{i,\lambda_0} \chi_i^{T} \Psi_T^{\lambda_0} \zeta_{T,j}^{\lambda_0} & \text{(active)} \end{cases} \tag{11}$$

In these equations, e_{λ_0} is the total energy delivered by the irradiation source at wavelength λ_0; Φ_i^{IFOV} is the fraction of that energy which is directed at the IFOV; $r_i^{2}\, \Omega_i^{IFOV}$ is the area corresponding to the IFOV at the scene; $\Psi_T^{\lambda_0}$ and $\Psi_B^{\lambda_0}$ are the target and background efficiencies to convert incident irradiation to fluorescence, respectively; $\zeta_{T,j}^{\lambda_0}$ and $\zeta_{B,j}^{\lambda_0}$ are the normalised fluorescent profile of the target and the background, respectively; t_{i,λ_0}^{a} is the transmission of the atmosphere at λ_0; $I_{i,j}$ is the averaged natural spectral radiant flux; $R_{i,j}^{T}$ and $R_{i,j}^{B}$ are the averaged spectral reflectance of the target and the background, respectively. Q_{i,λ_0}, referred to as the irradiation parameter, represents the total artificial radiant energy available for fluorescence conversion at position i. χ_i^{T} is the fraction of the dynamic FOV contained within the target FOV. This parameter is useful to

explore the detection capability of the instrument as a function of the scanning rate of the scene. χ_i^T is introduced to take into account a post-processing of the raw image to optimise the detection capability of the instrument for a target of interest. The post-processing referred to here is the convolution of the raw image with a window having the size of the target of interest. This is equivalent to binning the spatial pixels and the associated spectral equivalents of the 3D raw image obtained with the push broom imaging process. For $\chi_i^T > 1$ (case where the dynamic FOV is smaller than the target FOV), the signal increases through the convolution process. Furthermore, for this case, the fraction of signal originating from the background, χ_i^B, is approximated as zero[2]. For $\chi_i^T < 1$ (case where the dynamic FOV is larger than the target FOV), the signal from the target is not enhanced by the convolution process and an important contribution to the collected signals originates from the background materials. For that case, $\chi_i^B + \chi_i^T = 1$.

4.0 SIGNAL-TO-NOISE FUNDAMENTALS

In the previous chapter, a model has been developed to quantify the signal and the noise associated with active and passive imaging systems similar to the intensified CASI. These results will now be combined to form an expression equivalent to the usual signal-to-noise ratio (SNR) but specific to hyperspectral imaging systems. The goal is to provide a tool to predict the detection/identification capabilities of a hyperspectral imaging system for different scenarios in which parameters such as those identified in the previous chapter are known. The SNR is defined as the ratio of Equation 5 to the square root of Equation 6. Here, Equation 5 is modified by first neglecting the self-emission of the photocathode and by replacing $E_{i,j}^{SC}$ in the definition of $n_{i,j}^{SC}$ by $E_{i,j}^{T}$, thus giving $n_{i,j}^{T}$. Under intensified imaging operation where a high gain ($\eta_{i,j}^{CCD}\ T_{i,j}^{FB}\ \eta_{i,j}^{PS}\ G_{i,j} k >> 1$)[3] is

[2] This is not completely true because the dynamic FOV, even if smaller than the target FOV, may include a non negligible background signal. This off-target contribution may become critical if the fluorescence conversion efficiency of the background is much higher than the target itself. But, for the investigation goals pursued here and to keep the problem to an acceptable level of complexity, this zero approximation is applied. Readers should be aware of the consequences of this approximation.

[3] These conditions of operation are not that uncommon with an intensified hyperspectral camera based on a push broom acquisition process. The fact that the integrated signal originates from a single line at the scene and is distributed over the whole CCD array makes high gain possible without saturation of pixel-well capacities.

used and where the integrated spontaneous emission from the photocathode is negligible in comparison with the photons incident from the scene ($\varepsilon_{EBI}\Delta t << \eta_{i,j}^{PC} n_{i,j}^{SC}$ or $\eta_{i,j}^{PC} n_{i,j}^{T}$), $SNR_{i,j}$ is reduced to $n_{i,j}^{T}\sqrt{\eta_{i,j}^{PC}/k\, n_{i,j}^{SC}}$. For active imaging applications where the range-gated operation makes passive signals negligible, $SNR_{i,j}$ is developed further using Equations 10 and 11 as

$$SNR_{i,j} = \chi_i^T \Psi_T^{\lambda_0} \zeta_{T,j}^{\lambda_0} \sqrt{\eta_{i,j}^{PC} Q_{i,\lambda_0} C_{i,j} / k(\chi_i^T \Psi_T^{\lambda_0} \zeta_{T,j}^{\lambda_0} + \chi_i^B \Psi_B^{\lambda_0} \zeta_{B,j}^{\lambda_0})}. \quad (12)$$

This equation gives the signal-to-noise ratio for a look direction i and a spectral interval j as a function of the fluorescence characteristics of the target and the background, and as a function of the irradiation and the collection efficiencies of the imaging system. As for most SNR analyses, the signal of interest needs to be uncoupled from the background signals to make this equation of any practical use. For common applications, this uncoupling may be done by time or spatial unmixing (lock-in detection, heterodyne detection, etc.). For hyperspectral imaging, the uncoupling is performed using multivariate data analysis. The ability to do this is in fact what makes hyperspectral imaging so attractive for surveillance applications. The multivariate data analysis allows one to express the spectral profile obtained from a given look direction as a linear combination of spectral profiles associated with the different materials contained within the corresponding dynamic FOV. Furthermore, because most multivariate analyses exploit a statistical method based on least square modelling, if the spectral profile associated with the background material is (sufficiently) linearly independent from the one associated with the target, it is possible to define SNR_i, the signal-to-noise ratio associated with the probability of detection of a given target within look direction i, as

$$SNR_i = \sum_j S_{i,j} \Big/ \sqrt{\sum_j \langle N_{i,j}^2 \rangle} =$$

$$\chi_i^T \Psi_T^{\lambda_0} \sum_j \eta_{i,j}^{PC} C_{i,j} \zeta_{T,j}^{\lambda_0} \sqrt{Q_{i,\lambda_0} \Big/ k(\chi_i^T \Psi_T^{\lambda_0} \sum_j \eta_{i,j}^{PC} C_{i,j} \zeta_{T,j}^{\lambda_0} + \chi_i^B \Psi_B^{\lambda_0} \sum_j \eta_{i,j}^{PC} C_{i,j} \zeta_{B,j}^{\lambda_0})}. \quad (13)$$

This equation provides an important tool to predict the detection/identification performance of a target with an active hyperspectral imaging technique. As the linear dependence between the target and the background spectral fluorescent contributors

approaches zero (orthogonal condition), the numerical values obtained with Equation 13 can be closely related to a measure of probability similar to classical signal-to-noise analyses.

5.0 ABSOLUTE CALIBRATION OF THE INTENSIFIED CASI

With the intensified CASI, the coefficients relating the spectral radiant energy of the scene and the signal detected at the CCD must be evaluated in order to obtain quantitative information describing the physical characteristics of different materials of interest. For that purpose, a calibrated integrating sphere equipped with a variable attenuator was used.

The variable attenuator is composed of 21 discrete diaphragms of decreasing diameters. This approach has the advantage of reducing the exit radiance while minimising spectral profile variations between attenuation levels. For the two largest diaphragms (irises 1 and 2), the radiance has been calibrated independently. We have verified experimentally that the normalised spectral profiles is constant for these two irises. This spectral consistency is also assumed for other diaphragm sizes. An adjustable calibrated radiance source is thus obtained by measuring the scaling factors associated with the different diaphragm diameters. This has been done using the intensified CASI as a radiometer. Hyperspectral images of the integrating sphere exit window were taken for the first five consecutive sizes of diaphragm (irises 1 to 5) while keeping constant the numerical aperture of the camera (F#=1.4) and the intensifier gain. The same process was repeated but at a different intensifier gain level for irises 4 to 8, and three other times to cover all the 21 diaphragms. The five intensifier gain levels used throughout that process are 112, 147, 185, 220 and 255. In this study, the spatial non-uniformity of the intensifier gain is assumed to be independent of the level of amplification (future studies with the instrument should check this assumption). This reduces the gain of the MCP (G_{ij}) to G, a simple scaling parameter. With this approximation, the hyperspectral images of the exit window can be averaged to reduce the acquired information to a single spectral profile for each iris level.

Two types of information are deduced from these measurements. First, the scaling factors for the set of iris are derived relative to iris 1 (one of the two irises independently calibrated) by averaging the ratios of spectral profiles. Second, the five intensifier gains are quantified relative to the gain level value of 112. This set of scaling factors and relative intensifier gains is shown in Figure 3. A good linear relation on a logarithm plot is observed between the integrating sphere scaling factors and the selected diaphragms until iris 10 is reached. Discrepancies of unknown origin are observed for irises 11 and 12. A saturation is also observed for irises greater than 13, which is believed to be the result of the photocathode self-emission. The logarithm plot of the intensifier gains shows also a good linear relation with the 8-bit register intensifier gain level and a saturation is observed, as expected, for levels greater than 220.

The radiometric calibration of the intensified camera consists in experimentally measuring the spectral radiometric coefficients ($SRC_{i,j}$) that relate the number of electrons generated at the pixels of the CCD to a given spectral radiant energy collected at the scene. Based on the model developed in Chapter 3, the $SRC_{i,j}$ are defined as

$$SRC_{i,j} = n_{i,j}^{CCD} \Big/ E_{i,j}^{SC} = \pi/4 \, \eta_{i,j}^{CCD} T_{i,j}^{FB} \eta_{i,j}^{PS} \eta_{i,j}^{PC} A_i^{IFOV} t_{i,j}^{o} \eta_{i,j}^{s} t_{i,j}^{o} \frac{G_{i,j}}{F\#^2} = F_{i,j} \frac{G}{F\#^2}. \qquad (14)$$

In this equation, the self-emission of the photocathode is neglected and the parameters of the camera that cannot be altered by the user[4] have been grouped within a single array of parameters, $F_{i,j}$. On the other hand, G and F# are variable parameters set by the user and must be characterised to define adequately the $SRC_{i,j}$. Because the absolute value of the gain is a parameter difficult to obtain, it was chosen, for a constant F#, to define the $SRC_{i,j}$ as a function of G in a relative manner as

$$SRC_{i,j}^{N} = SRC_{i,j}^{R} \left(G^{N} / G^{R} \right), \qquad (15)$$

where N identifies the intensifier gain level for which the $SRC_{i,j}$ is required and R identifies the intensifier gain level for which a $SRC_{i,j}$ of reference has been measured. The ratio G^N/G^R is obtained from the plot of the relative intensifier gain found in Figure 3. The experimental measurement of $SRC_{i,j}^{R}$ is derived following a method similar to the

one given in Reference 8. This calibration process has been repeated for three intensifier gain levels (110, 125, 135 with F#=1.4). The result was three matrices of 512 columns and 288 rows. To test the proposed method taking into account the variability of the intensifier gain in the definition of spectral radiometric coefficients, the matrix with a gain of 110 was extrapolated from the ones obtained with gains of 125 and 135 using Equation 15 and compared with the one obtained experimentally. Figure 4 shows the column 256 of the matrix acquired experimentally with an intensifier gain level of 110 and the ones predicted from measurements taken with intensifier gain levels of 125 and 135. This result shows the limit of accuracy associated with a linear correction applied with a logarithmic dependent parameter. Two methods are proposed to improve this accuracy. First, a calibration target may be placed at the scene when this is possible. Second, several $SRC^{R}_{i,j}$ can be measured experimentally at closely spaced intensifier gain level intervals in order to minimise extrapolation errors. It is also important to note that the ripples observed in the plot of Figure 4 are in large part due to fixed pattern noise.

6.0 FLUORESCENT CHARACTERISTICS OF TYPICAL SURROGATE MINES

In order to predict the capabilities of detecting/identifying surface-laid mines using an active hyperspectral imaging technique, the fluorescence quantum yield ($\Psi_T^{\lambda_a}$) and spectral profile ($\zeta_{T,j}^{\lambda_a}$) of the targets of interest must be determined. This has been conducted in laboratory with a cotton glove (for comparison), three antitank surrogate mines (TMN-46, PM-60, TMB-D) and three antipersonnel surrogate mines (PNM-6, OZM-3, PFM-1)[5]. The intensified CASI was range-gated (100 ns gate width) and synchronised with excimer laser pulses (wavelength: 308 nm, pulse width: <20 ns, maximum repetition rate: 100 Hz). By changing the time delay of the gate, it was verified that the response time of the fluorescence was well within the 100 ns collection window. The targets, installed at a range of 2.6 m in a dark room, were irradiated in flood mode (no synchronous scanning). Depending on the fluorescence efficiency of the target, the

[4] For most scenarios of interest in the visible spectra, the range between the scene and the camera is assumed sufficiently short to approximate the transmission of the atmosphere as one. If this is not the case, the $SNR_{i,j}$ must be modified accordingly.

specific intensity of the radiant energy delivered at the scene was changed by using a lens and adjusting the laser pulse frequency. During these measurements, good care was taken to minimise thermal effects on the fluorescence properties of the targets by limiting the continuous irradiation periods. The laser spatial density of radiant energy at the scene ($e_{\lambda_i} \Phi_i^{IFOV} / r_i^2 \Omega_i^{IFOV}$ in Equation 10) was derived from a power meter placed at the scene for wide angular irradiation, and by characterising the spatial distribution and total power of the laser beam for narrow angular irradiation. To keep all backscattered light from entering the camera, a spectral filter made of an uncoated Lexan® plate was placed in front of the collecting lens. This filter has an optical transmission below $2x10^{-5}$ between 300 and 380 nm, and of about 0.9 (approximately uniform) between 400 and 900 nm. The scene with the irradiated targets was scanned by panning the range-gated intensified camera with a F# of 1.4 and an integration period of about 150 ms. The panning speed was adjusted to keep an aspect ratio of 1/1. The gain of the intensifier was adjusted after maximising the repetition rate of the laser in order to fill about ¾ of the 12-bit dynamic range of the CCD readout electronics. For each acquisition, the hyperspectral images are calibrated with the $SRC_{i,j}^{N}$ derived from Equation 15 where the $SRC_{i,j}^{R}$ with gain levels 110 ,125 and 135 mentioned in the previous chapter are used as reference. The resulting matrices are the specific intensity of the spectral radiant energy of the scene. From these data, quantum yields and spectral profiles are derived for the targets of interest with Equation 11. Figure 5 shows the fluorescent profile and quantum yield of a white cotton glove obtained in this manner. A section of 10x10 dynamic FOVs on target are averaged before deriving these fluorescent properties. The high value of the derived quantum yield (0.69) is consistent with the starch blanching process applied to this cotton fabric. The fluorescent spectra is centred at 440 nm with a width of 55 nm. The lobe around 900 nm results from the second-order of diffraction of the camera grating. However, the amplitude of this lobe does not reflect the diffraction efficiency of this second order because of the correction applied with the calibration process. A comparison of the ratio between the first and second diffraction efficiencies before calibration and for radiation at 450 nm shows an amplitude greater than 100. Similar measurements were made with the

[5] Surrogate manufacturer: Miltra Engineering Ltd, 357 Uxbridge Road, Rickmansworth, Herts, WD3 2DT, England.

mine surrogates and are shown in Figure 6. Because of the low quantum yields observed with these targets, no lens was placed into the laser path to reduce the irradiance at the scene. The peak irradiance was derived from the power and the size of the laser beam. Because of the smaller size of the non-diffracted laser beam, only a 3x3 section of dynamic FOVs at peak irradiance were averaged to derive the fluorescent characteristics. The quantum yields vary from a minimum of 3.4×10^{-5} for the TMN-46, a painted metallic antitank mine, to a maxima of 3.3×10^{-4} for the PNM-6, an antipersonnel mine with a rubber cover. Except for the PFM-1, each of these profiles shows a single smooth lobe of fluorescence with maximums between 450 and 550 nm and widths at half maximum between 150 and 210 nm. On the other hand, the fluorescent profile of the PFM-1 is composed of two lobes with one particularly narrow and centred at 560 nm. These fluorescent characteristics will be used in the following chapter for modeling.

7.0 SURFACE-LAID MINES DETECTION MODELLING

Based on the model developed in Chapters 3 and 4, and the fluorescent characteristics of typical surrogate mines obtained in Chapter 6, a scenario involving the detection of surface-laid mines from an airborne platform is investigated. In addition to the information listed in Table I, the following parameters are used for this investigation. The platform is positioned at an altitude of 300 m and the attenuation coefficients of the atmosphere are 0.2 km^{-1} (400-900 nm) and 0.5 km^{-1} (308 nm). The F# is 2.5, the camera integration period is 50 ms and the laser power is 10 W. The quantum efficiency of the photocathode is approximated as flat and equal to 0.1 in the spectral interval of interest. A quantum yield of 0.1 (worst-case scenario) is associated with background materials (vegetation) and 50 % of this parasitic fluorescence is localised within the fluorescent spectra of interest. The irradiation energy is distributed along a scanning line of 100 dynamic FOVs and the aspect ratio of these dynamic FOVs is 1:1. The TMN-46 antitank surrogate, with a quantum yield of 3.4×10^{-5} and a fluorescent profile given in Figure 6, is selected as the target of interest. The selection of this target sets the spectral interval of interest to ~400-700 nm and the target FOV to ~0.3x0.3 m^2 at a range of 300 m. With these parameters and the assumption that the intensified camera operates under photon

shot noise, it is now possible to use Equation 13 to evaluate the overall signal-to-noise ratio expected as a function of χ_i^T, the ratio between the target FOV and the dynamic FOV. This plot, shown in Figure 7, predicts a linear dependency of SNR_i with $\chi_i^T > 1$. It also shows that a highly fluorescent background contributing to the collected signal ($\chi_i^T < 1$) drastically reduces this ratio. The area scanning speed, given as the product of the number of look directions times the solid angle of the dynamic FOV divided by the camera integration time, is also plotted in this figure as a function of χ_i^T. Based on this plot, a signal-to-noise of about 3 is expected for an area scanning speed of 30 m^2/s. Given this signal to noise and by supposing an ideal linear independence between the fluorescent signature of the target in comparison with the background material[6], this result predicts a false alarm rate which will make this detection scenario difficult to apply.

8.0 CONCLUSION

An intensified hyperspectral camera is presented and described. Results of the radiometric calibration of the instrument are presented. A model based on a signal-to-noise ratio analysis is developed to evaluate the detection/identification capabilities of this instrument when used as a passive or an active hyperspectral imager. Then, this model is applied to the measurement of the hyperspectral signatures of laser-induced fluorescence from surface-laid mines from an aerial platform. Based on the fluorescent characteristics of the mine surrogates measured in the laboratory and other relevant parameters, a signal-to-noise ratio of 3 is predicted for an area scan speed of 30 m^2/s (TMN-46 antitank surrogate). This preliminary result indicates that the false alarm rate associated with this scenario of detecting surface-laid mines might be too high for a ground area scanning speed of practical interest.

[6] This allows the interpretation of the S/N with a statistics approaching a normal distribution.

9.0 REFERENCES

1. K. Staenz, J.C. Deguise, J. Schwarz, R. Brown, and T. Szeredi, "Overview of ISDAS Hyperspectral Information Extraction Techniques with Focus on Agricultural Applications", *4th International Symposium on Spectral Sensing Research (ISSSR)*, San Diego, CA, December 13-19, 1997.
2. S. Tompkins, J.M. Sunshine, and R.G. Resmini, "Terrain Categorization based on Classification of Results from Spectral Mixture Analysis on Hyperspectral Imagery", *4th International Symposium on Spectral Sensing Research (ISSSR)*, San Diego, CA, December 13-19, 1997.
3. A.J. Garrett, J.M. Irvine, T.K. Evers, J. Smyre, A.D. king, C. Ford, and D. Levine, "An imagery-Based Hydrodynamic Simulation of Effluent Streams Entering the Clinch River", *4th International Symposium on Spectral Sensing Research (ISSSR)*, San Diego, CA, December 13-19, 1997.
4. S.B. Achal, J.E. McFee and C.D. Anger, "Identification of surface-laid mines by classification of compact airborne spectrographic imager (casi) reflectance spectra", SPIE Vol. **2496**, p.324, 1995.
5. J.E. McFee and Herb T. Ripley, "Detection of buried landmines using a casi hyperspectral imager", SPIE Vol. **3079**, p.733, 1997.
6. M.K. Hamilton and W.E. Roper, "The U.S. Army's Center of Excellence for Spectral Sensing Technology", SPIE Vol. **3718**, p. 490, 1999.
7. J.W. Eastes, "Application of Multispectral Thermal Infrared Data to Military Problems: Discriminating Critical Targets and Decoys on the Battlefield", *4th International Symposium on Spectral Sensing Research (ISSSR)*, San Diego, CA, December 13-19, 1997.
8. S.K. Babey and R.J. Soffer, *"Radiometric calibration of the compact airborne spectrographic imager (CASI)"*, *Canadian Journal of Remote Sensing*, Vol. **18**, No. 4, Oct. 1992, p. 233.
9. S.K. Babey, C.D. Anger, S.B. Achal, T. Ivanco, A. Moise, P.R. Costella and J. DeBlick, "Development of a Next-Generation Compact Airborne Spectrographic Imager: casi-2", *4th International Airborne Remote Sensing Conference and Exhibition/21th Canadian Symposium on Remote Sensing*, Ottawa, Ontario, Canada, 21-24 June 1999.
10. Gerald C. Holst, *CCD arrays, cameras, and displays*, JCD Publishing, Winter Park, FL, and SPIE Optical Engineering press, Bellingham, Washington, USA, 1996.
11. Y.Talmi, *'Intensified Array Detectors"*, In *Charge-Transfer Devices in Spectroscopy*, J. V. Sweedler, K. L. Ratzlaff, and M. B. Denton, eds., Chapter 5, VCH Publishers, New York, 1994.

10.0 FIGURES AND TABLES

TABLE I

Parameters associated with the intensified camera. These parameters are either measured in the laboratory, derived from manufacturer specifications and public literature, or based on reasonable assumptions.

Parameters of the camera	Specifications	Parameters of the camera	Specifications
Focal length	11.2 mm	F#	1.4 – 16
Optical transmission	0.9	Grating efficiency	0.5 (max.)
Pixel-well capacity	300ke$^-$	Pixel size (w×L)	15×22.5 μm^2
Equivalent background illuminance (EBI)	0.17 μlux	Dark current	0.11 Digital Number/ms/pixel
Noise floor	50 e$^-$ (5°C)	CCD quantum efficiency	0.4 (@650 nm)
Photocathode quantum eff.	0.2 (S20, 450 nm)	Max. spectral resolution	~3 nm (@555 nm)

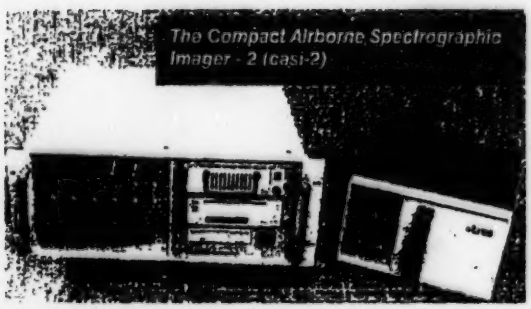

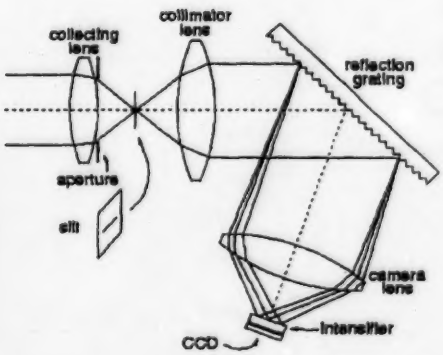

FIGURE 1 - The intensified Compact Airborne Spectrographic Imager (CASI). Shown are the PC-based control module and the camera head; the system is also composed of an intensifier power supply, a monitor and a keyboard (not shown). This is a second generation of CASI in which the original system has been modified by inserting an intensifier as depicted in the schematic diagram of the internal optics of the camera head (right).

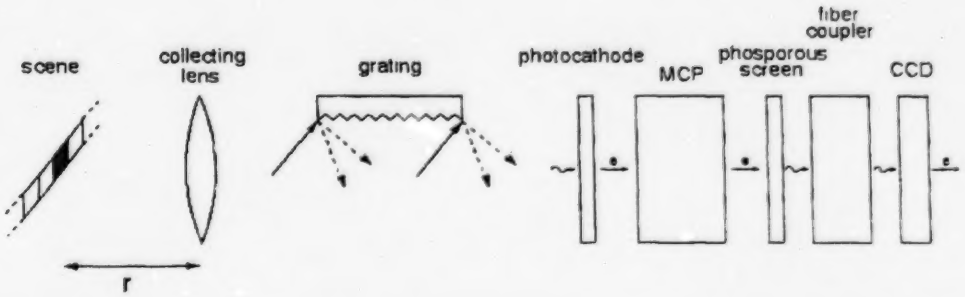

FIGURE 2 - Schematic representation of the different stages passed through by the collected signal before reaching the CCD

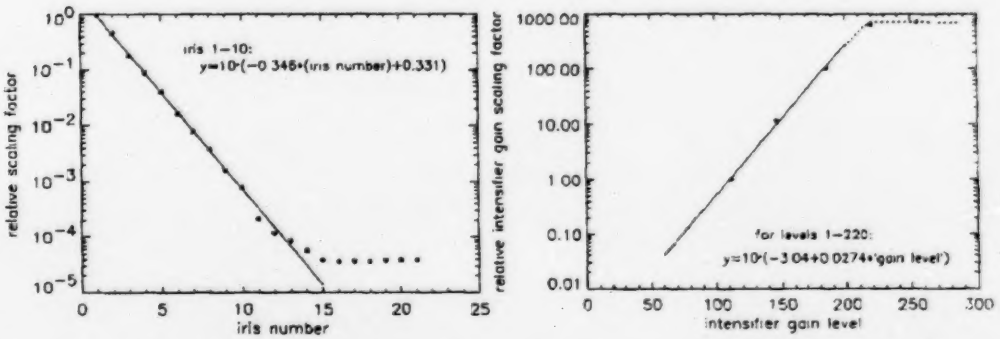

FIGURE 3 - Plot of the relative scaling factor of the integrating sphere as a function of the iris number (left). This plot was used to perform a spectral radiometric calibration of the intensified CASI. The saturation observed for iris numbers greater than 15 is associated to the self-emission of the photocathode. The relative plot of the intensification as a function of the gain level is shown on the right. A saturation of the intensification is observed for gain levels greater than 220.

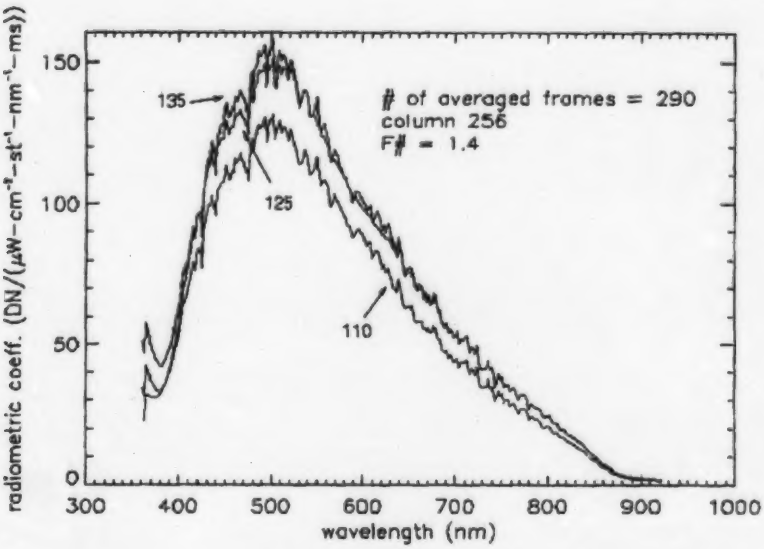

FIGURE 4 - Plot of the radiometric sensitivity coefficients of the intensified hyperspectral camera for a gain level of 110. The two other radiometric curves are predictions for a gain level of 110 derived from measurements made at gain levels 125 and 135. Scaling factors obtained from Figure 3 are used for these predictions.

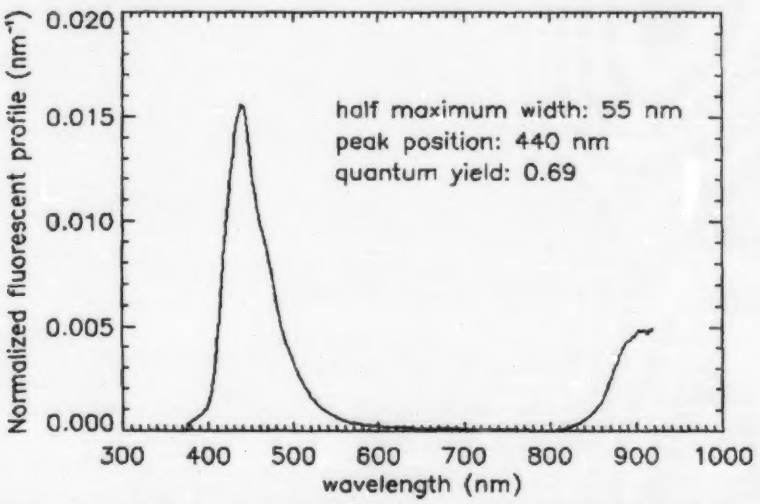

FIGURE 5 - Plot of the normalised fluorescent spectral profile of a white cotton glove when irradiated with laser light at 308 nm. The signal around 900 nm is associated with the second order of diffraction of the hyperspectral camera grating.

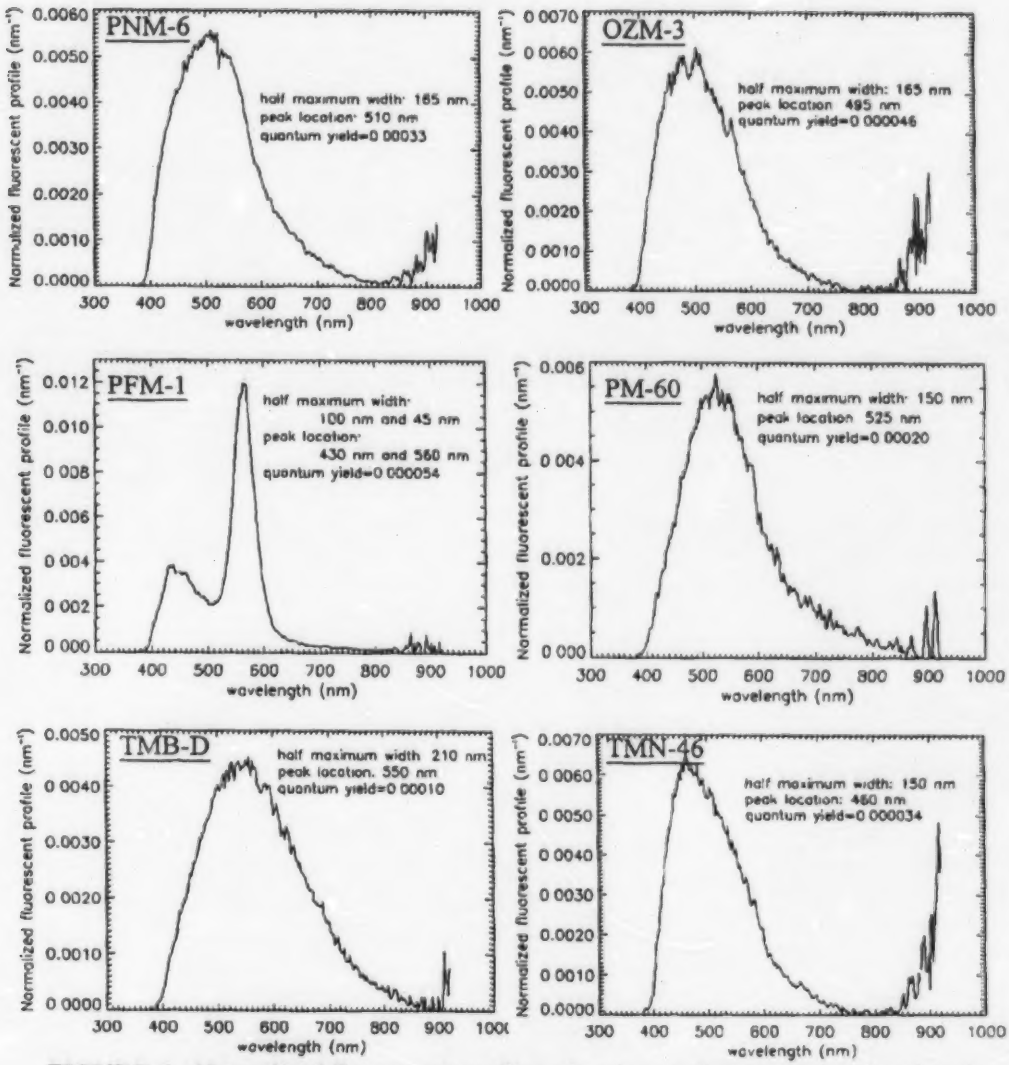

FIGURE 6 - Normalised fluorescent profiles of various anti-personnel and anti-tank mine surrogates. These profiles were corrected for the spectral radiometric response of the camera before being normalised. Irradiation is at 308 nm.

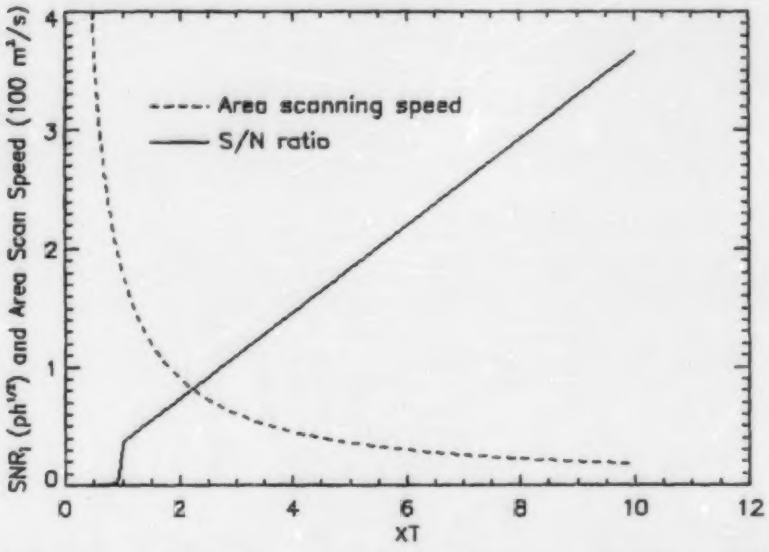

FIGURE 7 - Projected signal-to-noise ratio for the detection of surface-laid mines and the associated area scanning speed as a function of χ^T, the number of dynamic FOV on the target. These results are obtained with the proposed model for an airborne search scenario and the fluorescence characteristics of the TMN-46 mine surrogate.

INTERNAL DISTRIBUTION

DREV TM-2000-032

1 – Director General
1 – Deputy Director General
1 – Chief Scientist
6 – Document Library
1 – J.-R. Simard (author)
1 – P. Mathieu (author)
1 – Georges Fournier (author)
1 – V. Larochelle (author)
1 – G. Otis
1 – C. Carrier
1 – J.-M. Garneau
1 – J.-P. Ardouin
1 – T. Smithson
1 – J.-M. Thériault
1 – P. Chevrette
1 – J. Dubois
1 – J. Cruickshank
1 – D. Dion
1 – G. Tardif
1 – D. Dubé
1 – J. Rapanotti
1 – A. Blanchard
1 – M. Lévesque

EXTERNAL DISTRIBUTION

DREV-TM-2000-032

1 – DRDCIM
1 – DRDCIM (unbound copy)
1 – DRDC
1 – John McFee (DRES)
1 – David Liang (DREO)
1 – DREA
1 – DREO
1 – DRES
1 – DCIEM
1 – DSTA
1 – DSTL
1 – DSTM
1 – DST CCIS
1 – DST CCIS-5
1 – DSTA 2
1 – DSTA 3
1 – DSTA 4
1 – DSTA 5
1 – DSTL 5
1 – DAR 2
1 – DAR 2-4
1 – DAR 2-3
1 – DLR
1 – DMSS
1 – J2-Imagery 2-2-5
1 – ITRES Research Limited
Suite 155, East Atrium 2635 – 37th Avenue NE
Calgary, Alberta, Canada T1Y 5Z6
Attn: Stephen Babey, Chief Engineer (author)

DOCUMENT CONTROL DATA

1 ORIGINATOR (name and address)	2. SECURITY CLASSIFICATION (including special warning terms if applicable)
Jean-Robert Simard, DREV	UNCLASSIFIED

3. TITLE (its classification should be indicated by the appropriate abbreviation (S, C, R or U)
A RANGE-GATED INTENSIFIED SPECTROGRAPHIC IMAGER AN INSTRUMENT FOR ACTIVE HYPERSPECTRAL IMAGING (U)

4. AUTHORS (Last name, first name, middle initial. If military, show rank, e.g. Doe, Maj. John E.)
Simard, Jean-Robert (DREV), Mathieu, Pierre (DREV), Larochelle, Vincent (DREV), Fournier, Georges (DREV) and S.K. Babey (ITRES Research Ltd.)

5 DATE OF PUBLICATION (month and year)	6a. NO. OF PAGES	6b. NO. OF REFERENCES
April 2000	28	11

7. DESCRIPTIVE NOTES (the category of the document, e.g. technical report, technical note or memorandum. Give the inclusive dates when a specific reporting period is covered.)
Memorandum

8. SPONSORING ACTIVITY (name and address)
DRDB

9a PROJECT OR GRANT NO. (Please specify whether project or grant)	9b. CONTRACT NO.
3da29	

10a. ORIGINATOR'S DOCUMENT NUMBER	10b. OTHER DOCUMENT NOS
	N/A

11. DOCUMENT AVAILABILITY (any limitations on further dissemination of the document, other than those imposed by security classification)

- [X] Unlimited distribution
- [ ] Contractors in approved countries (specify)
- [ ] Canadian contractors (with need-to-know)
- [ ] Government (with need-to-know)
- [ ] Defense departments
- [ ] Other (please specify)

12. DOCUMENT ANNOUNCEMENT (any limitation to the bibliographic announcement of this document. This will normally correspond to the Document Availability (11). However, where further distribution (beyond the audience specified in 11) is possible, a wider announcement audience may be selected.)

UNLIMITED

13. ABSTRACT (a brief and factual summary of the document. It may also appear elsewhere in the body of the document itself. It is highly desirable that the abstract of classified documents be unclassified. Each paragraph of the abstract shall begin with an indication of the security classification of the information in the paragraph (unless the document itself is unclassified) represented as (S), (C), (R), or (U). It is not necessary to include here abstracts in both official languages unless the text is bilingual).

Hyperspectral imaging has demonstrated impressive capabilities in airborne surveys, particularly for mineral and biomass characterisations. Based on this success, it is believed that other applications like search and rescue operations, and detection/identification of various ground military targets could greatly benefit from this technology. The strength of hyperspectral imaging comes from the access to another dimension of information: the spectral content of the detected return signal for each spatial pixel. In the case of conventional hyperspectral imaging, the return signal depicts the spectral reflectance of the day irradiance from the scene within the field of view of each pixel. However, by inserting a range-gated intensifier into a hyperspectral camera and by combining the camera with selected pulsed lasers, it becomes possible to relate the returned spectral information to specific light/matter interactions like induced fluorescence. This new technique may be referred to as "active hyperspectral imaging". Among its advantages, this approach is independent of the ambient lighting conditions and can be customised in excitation wavelengths. Moreover, by using a range-gated intensified camera, it is possible to survey limited areas with a significant increase in signal-to-noise ratio. A camera of this type has been built by our group in collaboration with private industry and is described in this paper. The internal design of the camera is discussed, new issues concerning the calibration of the camera are depicted and a model based on signal-to-noise ratio analysis is presented. From the fluorescent characteristics of surrogate land mines measured in the laboratory, this model is used to predict the capabilities of detecting surface-laid mines from an aerial platform.

14. KEYWORDS, DESCRIPTORS or IDENTIFIERS (technically meaningful terms or short phrases that characterize a document and could be helpful in cataloguing the document. They should be selected so that no security classification is required. Identifiers, such as equipment model designation, trade name, military project code name, geographic location may also be included. If possible keywords should be selected from a published thesaurus, e.g. Thesaurus of Engineering and Scientific Terms (TEST) and that thesaurus-identified. If it is not possible to select indexing terms which are Unclassified, the classification of each should be indicated as with the title.)

Hyperspectral, imaging, remote sensing, laser, intensifier, range-gating, fluorescence.

#513569